# Boosting quantum Monte Carlo and alleviating sign problem by Gutzwiller projection

Wei-Xuan Chang and Zi-Xiang Li [*]

*Beijing National Laboratory for Condensed Matter Physics and Institute of Physics,
Chinese Academy of Sciences, Beijing 100190, China
and University of Chinese Academy of Sciences, Beijing 100049, China*

We present a scheme for projective quantum Monte Carlo (QMC) simulation that combines unbiased zero-temperature (projective) determinant QMC with variational Monte Carlo based on the Gutzwiller projected wave function. This approach is dubbed as Gutzwiller-projection QMC. Our numerical results demonstrate that the use of the Gutzwiller projected trial wave function significantly accelerates the convergence of computational results, thereby greatly reducing computational time in the simulation. Moreover, we provide an illustrative example showing that the sign problem is substantially mitigated in the Gutzwiller-projection QMC. We believe that the Gutzwiller-projection QMC opens up another pathway for enhancing efficiency and alleviating the sign problem in QMC simulations of interacting fermionic systems.

## I. INTRODUCTION

Demystifying quantum many-body physics in strongly correlated systems holds central importance in modern condensed matter physics. Developing efficient numerical approaches to solve quantum many-body systems in more than one dimension is particularly crucial. Among various numerical algorithms for quantum many-body problems, quantum Monte Carlo (QMC) plays a vital role because it is unbiased and approximation free [1–6]. However, QMC encounters the infamous sign problem [7–10], which significantly hinders its application to many strongly correlated systems, such as the Hubbard model at generic fillings. Therefore, solving or alleviating the sign problem in quantum many-body models potentially featuring intriguing physics would lead to substantial progress in understanding the strongly correlated physics of quantum many-body systems [4,11–25].

On the other hand, even for a QMC simulation free from the sign problem, the computational complexity generally scales cubically with the system size in fermionic systems, significantly limiting the method's applicability to large fermionic systems [6]. Despite recent advancements in algorithms for fermionic QMC [26–28], simulations of interacting fermionic systems are typically much more resource intensive than those of spin or bosonic systems. Consequently, even when a simulation is free from the sign problem, it is extremely challenging to access the accurate properties close to the thermodynamic limit in addressing crucial issues such as quantum criticality [29–44] and competing ordering [45–49]. Hence, the development of powerful and highly efficient algorithms for interacting fermion models is of paramount importance.

To this end, we develop a scheme of QMC simulation called Gutzwiller-projection QMC to expedite the simulation and, more importantly, alleviate the sign problem in interacting fermionic models. The fundamental concept of the approach involves combining variational Monte Carlo (VMC) based on the Gutzwiller projected variational wave function [50–53] and intrinsically unbiased projective QMC (PQMC) [6,54]. We implement a mean-field wave function under Gutzwiller projection as the trial wave function and employ the standard procedure of PQMC to access the ground-state properties of an interacting Hamiltonian without involving any uncontrolled approximations. In the framework of the Hubbard-Stratonovich transformation utilized in PQMC, the optimal Gutzwiller projected variational wave function with the minimum energy is efficiently achieved. Compared with conventional PQMC simulations that use a Slater-determinant trial wave function, Gutzwiller-projection QMC requires a much smaller projection parameter to ensure the convergence of results, significantly reducing computational time. More crucially, systematic calculations in specific models reveal that the sign problem is greatly mitigated in Gutzwiller-projection QMC.

## II. METHOD

In this section, we briefly illustrate the methods of Gutzwiller-projection QMC, which combines VMC based on the Gutzwiller projected wave function and unbiased PQMC. The main scheme of Gutzwiller-projection QMC is illustrated in Fig. 1. To avoid complexity, we consider a typical wave function with on-site Gutzwiller projection to illustrate our strategy, $|\psi_G\rangle = e^{-g\sum_i n_{i\uparrow}n_{i\downarrow}}|\psi_M\rangle$, where $|\psi_M\rangle$ is the Slater-determinant wave function of mean-field order, and $e^{-gn_{i\uparrow}n_{i\downarrow}}$ represents the Gutzwiller projection with the projective parameter $g$. The first step is to minimize the ground-state energy in terms of the Gutzwiller projected variational wave

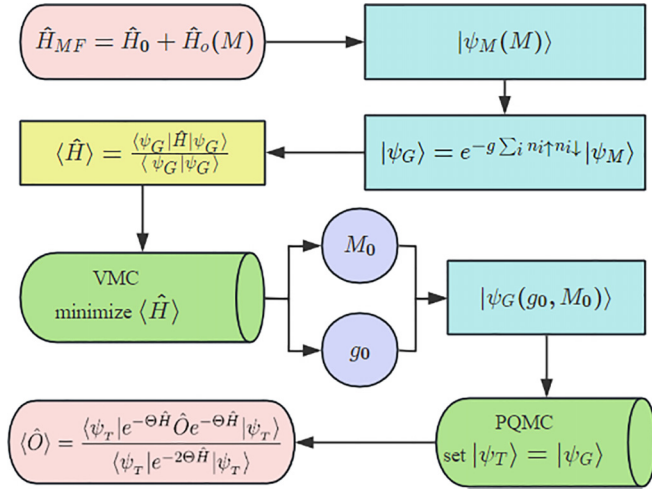[*]Contact author: zixiangli@iphy.ac.cn

FIG. 1. The flow chart of Gutzwiller-projection QMC, which illustrates the basic procedure of the approach schematically. The approach combines the VMC methods based on the Gutzwiller projected variational wave function and intrinsically unbiased PQMC approach, improving the efficiency and alleviating the sign problem in QMC simulation.

function. This process determines the optimal parameters for the projective parameter $g$ and the mean-field order parameter $M$ in the Slater-determinant wave function $|\psi_M\rangle$. Here, to calculate the expectation value of Hamiltonian, we perform the Hubbard-Stratonovich (HS) transformation on the Gutzwiller-projection term,

$$e^{-gn_{i\uparrow}n_{i\downarrow}} = \frac{1}{2}e^{-g/4}\sum_{s_i=\pm 1}e^{\lambda s_i(n_{i\uparrow}+n_{i\downarrow})}, \qquad (1)$$

where $\cosh\lambda = e^{\frac{g}{2}}$ and $s_i = \pm 1$ is the auxiliary field defined at each site $i$. Then the expectation value $\langle\hat{H}\rangle = \frac{\langle\psi_G|\hat{H}|\psi_G\rangle}{\langle\psi_G|\psi_G\rangle}$ is straightforwardly obtained using the standard procedure of PQMC. In Sec. I of the Supplemental Material (SM) [55], we present a detailed introduction to the PQMC algorithm for interacting fermionic systems. The reasons that we employ HS transformation on Gutzwiller terms are as follows: (1) The calculation of observables in terms of a Gutzwiller projected wave function through HS transformation is significantly faster than the conventional approach in VMC. This is because we only need to sample the configurations of discrete auxiliary fields. (2) More importantly, as we will illustrate later, the employment of HS transformation as presented in Eq. (1) enables the efficient simulation of PQMC involving projective imaginary-time evolution on a Gutzwiller projected trial wave function. As a result, after the HS transformation as shown in Eq. (1), we can identify the optimal parameters in the Gutzwiller projected wave function by minimizing the energy expectation value with high efficiency.

In the conventional PQMC algorithm, the ground-state expectation value of an observable $\hat{O}$ is evaluated as $\langle\hat{O}\rangle = \frac{\langle\psi_T|e^{-\Theta\hat{H}}\hat{O}e^{-\Theta\hat{H}}|\psi_T\rangle}{\langle\psi_T|e^{-2\Theta\hat{H}}|\psi_T\rangle}$, where $|\psi_T\rangle$ is the trial wave function, and typically, a Slater-determinant wave function to facilitate the simulation. Crucially, upon applying HS transformation on the Gutzwiller-projection term as described in Eq. (1), it is

feasible to use a Gutzwiller projected wave function as a trial wave function in PQMC. Hence, after obtaining the optimal values of $g$ and $M$ in the Gutzwiller projected wave function $|\psi_G\rangle$, we compute the expectation value of observables as $\langle\hat{O}\rangle = \frac{\langle\psi_T|e^{-\Theta\hat{H}}\hat{O}e^{-\Theta\hat{H}}|\psi_T\rangle}{\langle\psi_T|e^{-2\Theta\hat{H}}|\psi_T\rangle}$, employing the optimal Gutzwiller projected wave function as the initial trial wave function $|\psi_T\rangle = |\psi_G\rangle$. We implement the standard procedures of Trotter decomposition and HS transformation in PQMC and decouple the Gutzwiller-projection term using Eq. (1). Consequently, the ground-state expectation values of observables are easily accessed within the framework of the standard PQMC algorithm. Although the computational complexity is the same for conventional PQMC and Gutzwiller-projection QMC, we expect that the computational time is largely saved under the employment of the Gutzwiller projected state as the trial state, which reduces the projective imaginary-time $\Theta$ required for the convergence of observable.

## III. THE HONEYCOMB HUBBARD MODEL

To demonstrate the efficiency of Gutzwiller-projection QMC, we first apply the approach to the spin-1/2 Hubbard model [56] on a honeycomb lattice,

$$H = -t\sum_{\langle ij\rangle,\sigma}(c_{i\sigma}^{\dagger}c_{j\sigma} + \text{H.c.}) + U\sum_i\left(n_{i\uparrow} - \frac{1}{2}\right)\left(n_{i\downarrow} - \frac{1}{2}\right), \qquad (2)$$

where $c_{i\sigma}^{\dagger}$ creates an electron on site $i$ with spin polarization $\sigma = \uparrow/\downarrow$, $t$ is the nearest-neighbor (NN) hopping amplitude, and $U$ is the amplitude of on-site Hubbard repulsion. Hereafter, we set $t = 1$ as the unit of energy. We focus the study on half filling, where the sign problem is circumvented by choosing the appropriate HS transformation channel. In the noninteracting limit, namely $U = 0$, the model at half filling features Dirac fermions with Fermi energy located at the Dirac point. With increasing Hubbard interaction amplitude, a quantum phase transition between the Dirac semimetal (DSM) and the antiferromagnetic (AFM) Mott insulator occurs at $U = U_c \approx 3.85$, and the transition belongs to the chiral-Heisenberg universality class [57–61].

We implement the Gutzwiller-projection QMC algorithm to study the ground-state properties of Eq. (2) at half filling. Because AFM is the dominant instability in the model, it is natural to choose the AFM mean-field wave function with Gutzwiller projection as the trial wave function in the simulation,

$$|\psi_T\rangle = e^{-g\sum_i n_{i\uparrow}n_{i\downarrow}}|\psi_N\rangle, \qquad (3)$$

where $g$ is the parameter of the Gutzwiller projection and $\psi_N$ is the mean-field wave function featuring Néel AFM order. More explicitly, $\psi_N$ is generated as the ground-state wave function of the Hamiltonian $H_N = H_0 + M_N\sum_i(-1)^{\delta_i}(n_{i\uparrow} - n_{i\downarrow})$, where $H_0$ is the noninteracting part of Eq. (2), $M_N$ is the Néel AFM order parameter, and $\delta_i = \pm 1$ if site $i$ belongs to the A(B) sublattice. Employing the procedure introduced in the last section is straightforward to access the expectation value of energy in terms of the trial wave function Eq. (3) under the choice of $g$ and $M_N$. Figure 2 depicts the expectation value of energy with varying Néel order parameter $M_N$
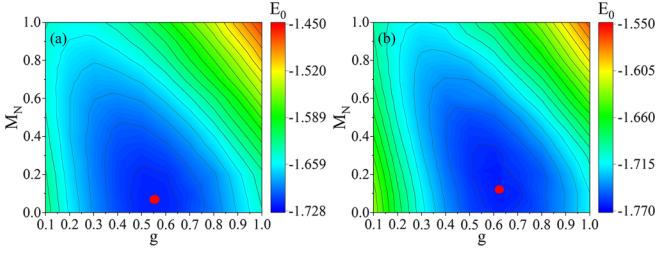
FIG. 2. The contour plot shows the energy vs variational parameters in the Gutzwiller projected wave function for (a) $U = 3.5$ and (b) $U = 4.0$. The parameters $(g, M_N)$ with minimum energy are indicated by the red circles. The optimal parameters are $g = 0.55$ and $M_N = 0.07$ for $U = 3.5$, and $g = 0.62$ and $M_N = 0.11$ for $U = 4.0$.

and Gutzwiller-projection parameter $g$ for different choices of Hubbard interaction strength $U = 3.5$ and $U = 4.0$ located in the DSM phase and AFM ordered phase, respectively. We obtain the optimal values of parameters $g$ and $M_N$ by minimizing the expectation value of Eq. (2) and achieving the trial wave function utilized in the PQMC simulation, as introduced in the last section.

We compare the convergence of results against the projection parameter $\Theta$ using distinct choices of trial wave functions. The ground-state energy and AFM structure factor (the definitions are shown in Sec. II of SM [55]) are evaluated versus $\Theta$, as depicted in Fig. 3. The results unambiguously demonstrate that accurate ground-state energy is achieved at a much smaller value of $\Theta$ in Gutzwiller-projection QMC compared to conventional PQMC simulations, which

use a Slater-determinant wave function as the trial wave function. In conventional PQMC simulations, two different Slater-determinant trial wave functions are employed: the ground-state wave function of the noninteracting part in Eq. (2) and the AFM mean-field wave function without Gutzwiller projection. The ground-state energy and AFM structure factor $S_{AFM}$ exhibit much slower convergence against the projection parameter $\Theta$ in both cases. Surprisingly, within the same number of Monte Carlo samplings, the statistical errors of observables are significantly reduced in Gutzwiller-projection QMC compared to conventional PQMC with a Slater-determinant trial wave function. The corresponding results of statistical error are included in Sec. III of the SM [55]. To further confirm the correctness of the approach, we perform an exact diagonalization (ED) calculation on model Eq. (2) and compare the results of Gutzwiller-projection QMC and ED, which exhibit perfect consistency and further demonstrate the correctness of our approach. The detailed results of ED are included in Sec. IV of the SM [55]. Moreover, to demonstrate the efficiency of the approach quantitatively, we perform a comparison of computational time used in Gutzwiller-projection QMC and conventional PQMC, as shown in Sec. V of the SM [55]. The results show that employing the Gutzwiller projected trial wave function reduces the computational time substantially.

## IV. REPULSIVE SPINLESS HONEYCOMB MODEL

For the honeycomb Hubbard model, we have demonstrated that employing the Gutzwiller projected trial wave function accelerates the convergence of results concerning the
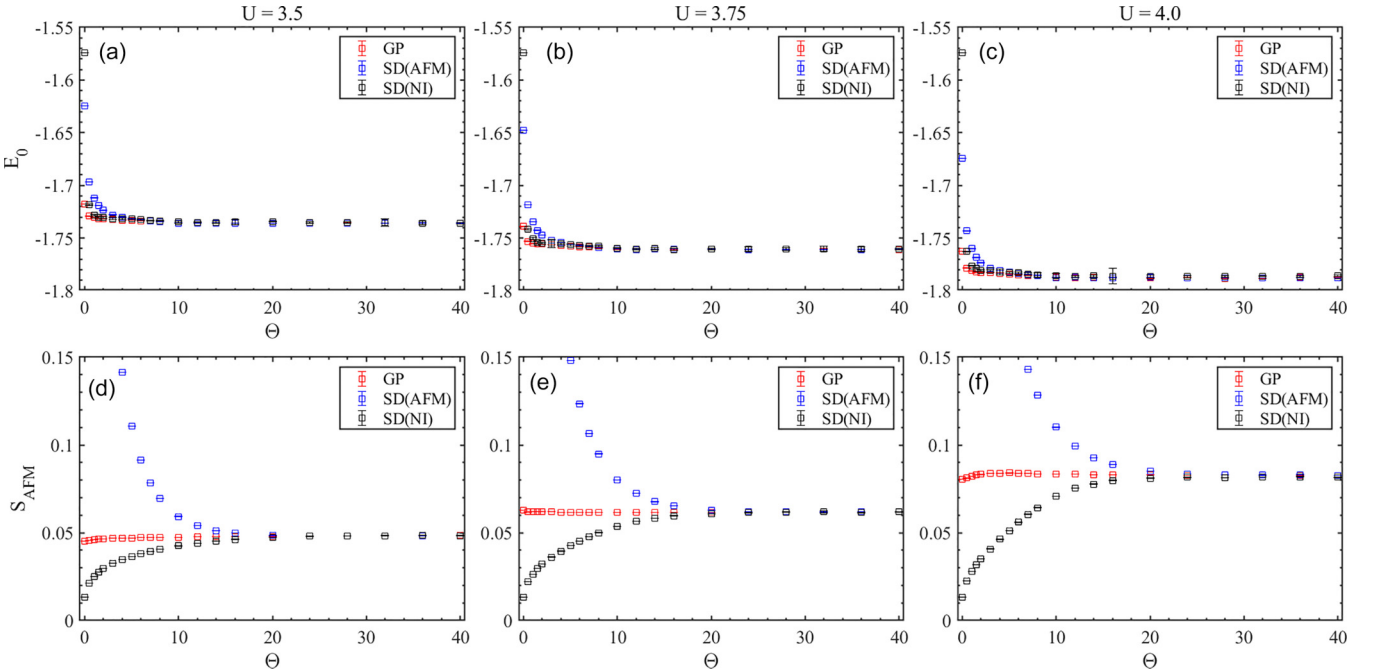


FIG. 3. The results of simulation on spinful Hubbard model at half filling for the Gutzwiller-projection QMC and the conventional PQMC with a Slater-determinant trial wave function. The results of ground-state energy vs projective parameter $\Theta$ for (a) $U = 3.5$, (b) $U = 3.75$, and (c) $U = 4$. The results of AFM structure factor $S_{AFM}$ vs projective parameter $\Theta$ for (d) $U = 3.5$, (e) $U = 3.75$, and (f) $U = 4$. GP, SD(AFM), and SD(NI) denote the results of the simulation employing the Gutzwiller projected wave function, AFM mean-field Slater-determinant wave function, and noninteracting Slater-determinant wave function as the trial wave functions, respectively.

projection parameter $\Theta$ significantly, thereby vastly improving the efficiency of QMC simulations. In this section, we apply Gutzwiller-projection QMC to the spinless $t - V$ model, specifically the model of spinless fermions with nearest-neighbor (NN) interactions on the honeycomb lattice. The Hamiltonian of the model is given by

$$H = -t \sum_{\langle ij \rangle} (c_i^\dagger c_j + \text{H.c.}) + V \sum_{\langle ij \rangle} \left( n_i - \frac{1}{2} \right) \left( n_j - \frac{1}{2} \right), \tag{4}$$

where $c_i$ is the annihilation operator of the fermion on site $i$, $t$ is the NN hopping amplitude, and $V > 0$ denotes the density repulsive interaction between NN sites. We focus on the model at half filling. The quantum phase diagram of the model at half filling has been extensively investigated in recent years, featuring a quantum phase transition from the DSM phase to the charge-density-wave (CDW) insulating phase with increasing NN density interaction strength [62,63]. The presence of the sign problem hinges on the schemes of the HS transformation. Simulation encounters the sign problem when the nearest-neighbor (NN) density interaction is decoupled in the hopping channel. Recent studies have revealed that despite the existence of the sign problem, the average sign exhibits two distinct behaviors in the weak- and strong-coupling regimes [64]. In the weak-coupling regime, the model is asymptotically sign free; namely, the average sign asymptotically increases to one as the system size increases. In contrast, in the strong-coupling regime, the average sign exhibits exponentially decaying scaling, consistent with the conventional scaling behavior of the sign problem in QMC simulations. Here, we decouple the interaction in the density channel and perform Gutzwiller-projection QMC simulation on the model, aiming to investigate the effect of the Gutzwiller projected trial wave function on the efficiency of the simulation and, more importantly, on the behavior of the sign problem.

In the simulation of the spinless honeycomb $t - V$ model, we choose the CDW mean-field wave function with Gutzwiller projection on the NN bond as the trial wave function,

$$|\psi_T\rangle = e^{-g \sum_{\langle ij \rangle} n_i n_j} |\psi_C\rangle, \tag{5}$$

where $g$ is the parameter of the Gutzwiller projection on NN bonds. $\psi_C$ is the mean-field wave function with CDW ordering, generated as the ground-state wave function of the mean-field Hamiltonian $H_C = H_0 + \Delta_C \sum_i (-1)^{\delta_i} n_i$, where $H_0$ is the noninteracting part in Hamiltonian Eq. (4), $\Delta_C$ is the CDW order parameter, and $\delta_i = \pm 1$ if site $i$ belongs to the A(B) sublattice. Similar to the spinful honeycomb Hubbard model, we access the optimal variational parameters $g$ and $\Delta_C$ by minimizing the expectation value of $H$ defined in Eq. (4). We perform a QMC simulation with the corresponding Gutzwiller projected trial wave function. The results of ground-state energy and CDW structure factor for several values of $V$, with the detailed definitions included in the SM [55], are presented in Fig. 4. These results explicitly demonstrate that a smaller value of $\Theta$ is sufficient to achieve accurate ground-state results of energy and the CDW structure factor in
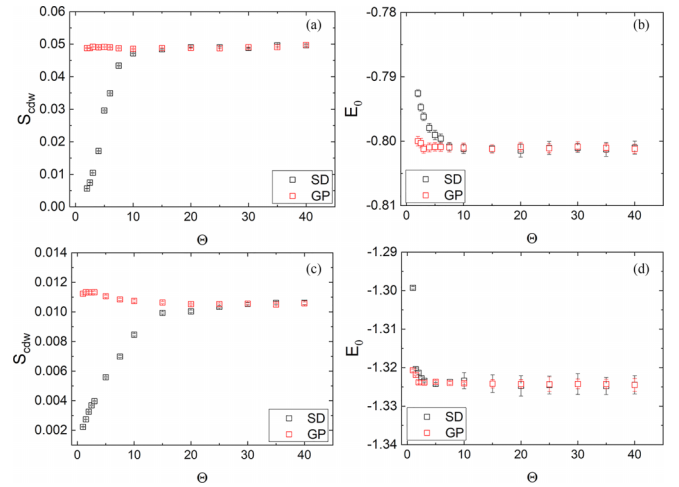


FIG. 4. The results of observables in the spinless $t - V$ model at half filling for Gutzwiller-projection QMC and conventional PQMC with a Slater-determinant trial wave function. The results of the CDW structure factor $S_{\text{CDW}}$ for (a) $V = 1.6$ and (c) $V = 1.35$. The results of ground-state energy $E_0$ for (b) $V = 1.6$ and (d) $V = 1.35$. SD denotes the results of conventional PQMC with the employment of a noninteracting Slater-determinant trial wave function, and GP denotes the results of Gutzwiller-projection QMC. The system size is fixed $L = 15$.

Gutzwiller-projection QMC. The improvement in efficiency is particularly pronounced in the CDW ordered phase ($V > V_c \sim 1.35$).

Then, we investigate the behavior of the sign problem in the Gutzwiller-projection QMC simulation. For simulation of Eq. (4) with HS transformation in the density channel, as aforementioned, the model is intrinsically sign problematic only when the interaction is strong ($V > V^* \sim 1.2$), whereas the model displays asymptotic sign-free behavior in the weak-coupling regime, namely the average sign increases and approaches one as the system size increases [64]. Hence, we focus on the strong-coupling regime where the sign problem is severe. We calculate the average sign as a function of the projective parameter $\Theta$ for $V = 1.35$ and $V = 1.6$, as depicted in Figs. 5(a) and 5(b), respectively. For comparison, we present the results of conventional PQMC with a Slater-determinant trial function generated as the ground state of the noninteracting part in Eq. (4). Intriguingly, the results show that the average sign is obviously increased in the simulation with the Gutzwiller projected trial wave function compared to the conventional PQMC with the Slater-determinant trial wave function. Hence, the sign problem is significantly alleviated in the Gutzwiller-projection QMC. Furthermore, we plot the average sign versus linear system size in the simulation of Gutzwiller-projection QMC and conventional PQMC for $V = 1.6$ [shown in Fig. 5(c)], which unequivocally demonstrates that the sign problem in the spinless honeycomb $t - V$ model at half filling is mitigated by employing the Gutzwiller projected trial wave function, particularly when the linear system size $L$ is large.
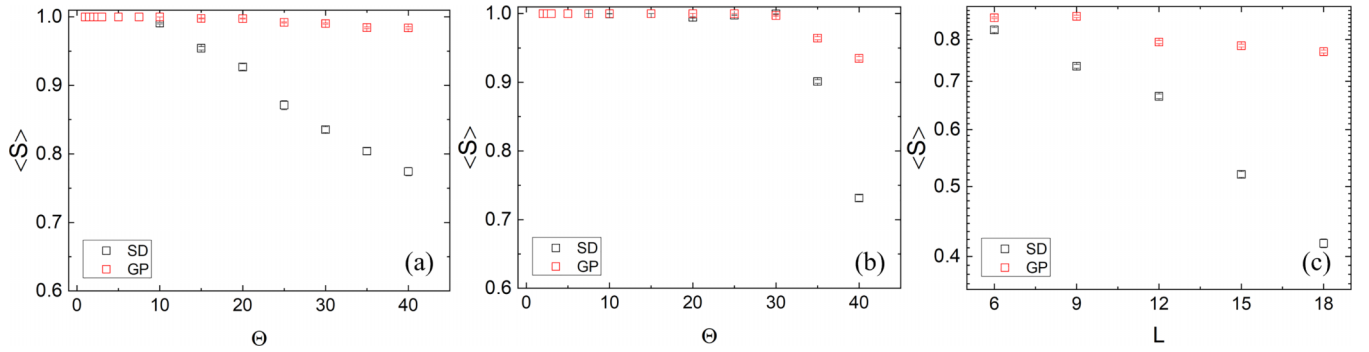
FIG. 5. The results of the sign problem in the spinless $t - V$ model at half filling for Gutzwiller-projection QMC and conventional PQMC with a Slater-determinant trial wave function. (a) The result of the sign problem vs the projective parameter $\Theta$ for $L = 15$ and $V = 1.6$. (b) The results of the sign problem vs the projective parameter $\Theta$ for $L = 15$ and $V = 1.35$. (c) The results of the sign problem vs linear system size $L$ for $V = 1.6$. SD denotes the results of conventional PQMC with the employment of a noninteracting Slater-determinant trial wave function, and GP denotes the results of Gutzwiller-projection QMC.

## V. DISCUSSIONS AND CONCLUDING REMARKS

We present numerical results that Gutzwiller projection significantly expedites the convergence against projection imaginary time and alleviates the sign problem in PQMC in several examples of strongly interacting fermionic models. Very recently, a similar approach has been applied in the Hubbard-related model and molecular systems [65–67]. In our work, we utilize the general form of Gutzwiller projection, and perform a more systematic investigation on the mitigation of the sign problem in a class of strongly interacting models through the application of the Gutzwiller projection and variational procedure on a trial wave function. We believe that it is straightforward to apply the approach to other classes of models. The reduction of projection imaginary time required for the convergence of results and mitigation of the sign problem relies on the fact that the Gutzwiller projected wave function with the appropriate choice of parameters is close to the true ground-state wave function of the Hamiltonian. Hence, our approach is applicable in cases in which a Gutzwiller projected wave function can qualitatively capture the correlation effect of the Hamiltonian and symmetry breaking in the ground state. For models in which it is difficult to capture the ground-state features through the Gutzwiiler projected mean-field wave function, whether the Gutzwiller-projection QMC can achieve an obvious improvement of efficiency is elusive. The systematic investigation of the applicability of the approach is left for future study.

In summary, we have developed a scheme of zero-temperature (projective) determinant QMC enhanced by Gutzwiller projection. To demonstrate its remarkable efficiency, we apply this approach to two typical quantum many-body models. In the spinful honeycomb Hubbard model, our results clearly demonstrate that crucial observables, such as the ground-state energy and the AFM structure factor, converge much faster for the projection parameter $\Theta$. This leads to a significant reduction in the computational time required to achieve the desired level of accuracy. Similarly, in the spinless honeycomb $t - V$ model, observables converge faster with a smaller projection parameter in Gutzwiller-projection QMC compared to the conventional PQMC algorithm. Moreover, the Gutzwiller-projection QMC simulation notably alleviates the sign problem of the model, particularly in regions where it is most severe. In conclusion, Gutzwiller-projection QMC presents a promising approach for accelerating simulations of ground-state properties in interacting fermionic models and alleviating the sign problem in QMC simulation.

[1] D. J. Scalapino and R. L. Sugar, Method for performing Monte Carlo calculations for systems with fermions, Phys. Rev. Lett. **46**, 519 (1981).

[2] J. E. Hirsch, D. J. Scalapino, R. L. Sugar, and R. Blankenbecler, Efficient Monte Carlo procedure for systems with fermions, Phys. Rev. Lett. **47**, 1628 (1981).

[3] S. R. White, D. J. Scalapino, R. L. Sugar, and N. E. Bickers, Monte Carlo calculation of dynamical properties of the two-dimensional Hubbard model, Phys. Rev. Lett. **63**, 1523 (1989).

[4] S. Zhang, J. Carlson, and J. E. Gubernatis, Constrained path quantum Monte Carlo method for fermion ground states, Phys. Rev. Lett. **74**, 3652 (1995).

[5] E. Gull, A. J. Millis, A. I. Lichtenstein, A. N. Rubtsov, M. Troyer, and P. Werner, Continuous-time Monte Carlo methods for quantum impurity models, Rev. Mod. Phys. **83**, 349 (2011).

[6] F. F. Assaad and H. G. Evertz, *Computational Many-Particle Physics* (Springer, Berlin, 2008), pp. 277–356.

[7] M. Troyer and U.-J. Wiese, Computational complexity and fundamental limitations to fermionic quantum Monte Carlo simulations, Phys. Rev. Lett. **94**, 170201 (2005).

[8] Z.-X. Li and H. Yao, Sign-problem-free fermionic quantum Monte Carlo: Developments and applications, Annu. Rev. Condens. Matter Phys. **10**, 337 (2019).

[9] E. Y. Loh, J. E. Gubernatis, R. T. Scalettar, S. R. White, D. J. Scalapino, and R. L. Sugar, Sign problem in the numerical simulation of many-electron systems, Phys. Rev. B **41**, 9301 (1990).

[10] R. Mondaini, S. Tarat, and R. T. Scalettar, Quantum critical points and the sign problem, Science **375**, 418 (2022).

[11] C. Wu and S.-C. Zhang, Sufficient condition for absence of the sign problem in the fermionic quantum Monte Carlo algorithm, Phys. Rev. B **71**, 155115 (2005).

[12] Z.-X. Li, Y.-F. Jiang, and H. Yao, Solving the fermion sign problem in quantum Monte Carlo simulations by Majorana representation, Phys. Rev. B **91**, 241117(R) (2015).

[13] Z.-X. Li, Y.-F. Jiang, and H. Yao, Majorana-time-reversal symmetries: A fundamental principle for sign-problem-free quantum Monte Carlo simulations, Phys. Rev. Lett. **117**, 267002 (2016).

[14] C. J. Umrigar, J. Toulouse, C. Filippi, S. Sorella, and R. G. Hennig, Alleviation of the fermion-sign problem by optimization of many-body wave functions, Phys. Rev. Lett. **98**, 110201 (2007).

[15] D. Hangleiter, I. Roth, D. Nagaj, and J. Eisert, Easing the Monte Carlo sign problem, Sci. Adv. **6**, eabb8341 (2020).

[16] Z.-Q. Wan, S.-X. Zhang, and H. Yao, Mitigating the fermion sign problem by automatic differentiation, Phys. Rev. B **106**, L241109 (2022).

[17] X. Zhang, G. Pan, X. Y. Xu, and Z. Y. Meng, Fermion sign bounds theory in quantum Monte Carlo simulation, Phys. Rev. B **106**, 035121 (2022).

[18] Y. Ouyang and X. Y. Xu, Projection of infinite-$U$ Hubbard model and algebraic sign structure, Phys. Rev. B **104**, L241104 (2021).

[19] L. Wang, Y.-H. Liu, M. Iazzi, M. Troyer, and G. Harcos, Split orthogonal group: A guiding principle for sign-problem-free fermionic simulations, Phys. Rev. Lett. **115**, 250601 (2015).

[20] Z. C. Wei, C. Wu, Y. Li, S. Zhang, and T. Xiang, Majorana positivity and the fermion sign problem of quantum Monte Carlo simulations, Phys. Rev. Lett. **116**, 250601 (2016).

[21] R. Levy and B. K. Clark, Mitigating the sign problem through basis rotations, Phys. Rev. Lett. **126**, 216401 (2021).

[22] S. Zhang, J. Carlson, and J. E. Gubernatis, Constrained path Monte Carlo method for fermion ground states, Phys. Rev. B **55**, 7464 (1997).

[23] M. Qin, T. Schäfer, S. Andergassen, P. Corboz, and E. Gull, The Hubbard model: A computational perspective, Annu. Rev. Condens. Matter Phys. **13**, 275 (2022).

[24] O. Grossman and E. Berg, Robust Fermi-liquid instabilities in sign problem-free models, Phys. Rev. Lett. **131**, 056501 (2023).

[25] A. Alexandru, G. Başar, P. F. Bedaque, and N. C. Warrington, Complex paths around the sign problem, Rev. Mod. Phys. **94**, 015006 (2022).

[26] Y.-Y. He, H. Shi, and S. Zhang, Reaching the continuum limit in finite-temperature *ab initio* field-theory computations in many-fermion systems, Phys. Rev. Lett. **123**, 136402 (2019).

[27] B. Cohen-Stead, O. Bradley, C. Miles, G. Batrouni, R. Scalettar, and K. Barros, Fast and scalable quantum Monte Carlo simulations of electron-phonon models, Phys. Rev. E **105**, 065302 (2022).

[28] L. Wang, M. Iazzi, P. Corboz, and M. Troyer, Efficient continuous-time quantum Monte Carlo method for the ground state of correlated fermions, Phys. Rev. B **91**, 235151 (2015).

[29] E. Berg, S. Lederer, Y. Schattner, and S. Trebst, Monte Carlo studies of quantum critical metals, Annu. Rev. Condens. Matter Phys. **10**, 63 (2019).

[30] E. Berg, M. A. Metlitski, and S. Sachdev, Sign-problem-free quantum Monte Carlo of the onset of antiferromagnetism in metals, Science **338**, 1606 (2012).

[31] X. Y. Xu, Z. H. Liu, G. Pan, Y. Qi, K. Sun, and Z. Y. Meng, Revealing fermionic quantum criticality from new Monte Carlo techniques, J. Phys.: Condens. Matter **31**, 463001 (2019).

[32] X.-J. Yu, Z. Pan, L. Xu, and Z.-X. Li, Non-Hermitian strongly interacting Dirac fermions, Phys. Rev. Lett. **132**, 116503 (2024).

[33] A. W. Sandvik, Evidence for deconfined quantum criticality in a two-dimensional Heisenberg model with four-spin interactions, Phys. Rev. Lett. **98**, 227202 (2007).

[34] H. Shao, W. Guo, and A. W. Sandvik, Quantum criticality with two length scales, Science **352**, 213 (2016).

[35] Z.-X. Li, Y.-F. Jiang, S.-K. Jian, and H. Yao, Fermion-induced quantum critical points, Nat. Commun. **8**, 314 (2017).

[36] F. F. Assaad and I. F. Herbut, Pinning the order: The nature of quantum criticality in the Hubbard model on honeycomb lattice, Phys. Rev. X **3**, 031010 (2013).

[37] Y. Schattner, S. Lederer, S. A. Kivelson, and E. Berg, Ising nematic quantum critical point in a metal: A Monte Carlo study, Phys. Rev. X **6**, 031028 (2016).

[38] X. Y. Xu, K. Sun, Y. Schattner, E. Berg, and Z. Y. Meng, Non-Fermi liquid at $(2+1)$D ferromagnetic quantum critical point, Phys. Rev. X **7**, 031058 (2017).

[39] Z.-X. Li, A. Vaezi, C. B. Mendl, and H. Yao, Numerical observation of emergent spacetime supersymmetry at quantum criticality, Sci. Adv. **4**, eaau1463 (2018).

[40] Y.-K. Yu, Z. Zeng, Y.-R. Shu, Z.-X. Li, and S. Yin, Nonequilibrium dynamics in Dirac quantum criticality, arXiv:2310.10601.

[41] Z. Zeng, Y.-K. Yu, Z.-X. Li, Z.-X. Li, and S. Yin, Finite-time scaling beyond the Kibble-Zurek prerequisite: Driven critical dynamics in strongly interacting Dirac systems, arXiv:2403.19258.

[42] J. Schwab, L. Janssen, K. Sun, Z. Y. Meng, I. F. Herbut, M. Vojta, and F. F. Assaad, Nematic quantum criticality in Dirac systems, Phys. Rev. Lett. **128**, 157203 (2022).

[43] F. F. Assaad and T. Grover, Simple fermionic model of deconfined phases and phase transitions, Phys. Rev. X **6**, 041049 (2016).

[44] S. Gazit, M. Randeria, and A. Vishwanath, Emergent Dirac fermions and broken symmetries in confined and deconfined phases of $Z_2$ gauge theories, Nat. Phys. **13**, 484 (2017).

[45] E. Fradkin, S. A. Kivelson, and J. M. Tranquada, Colloquium: Theory of intertwined orders in high temperature superconductors, Rev. Mod. Phys. **87**, 457 (2015).

[46] Y. Schattner, M. H. Gerlach, S. Trebst, and E. Berg, Competing orders in a nearly antiferromagnetic metal, Phys. Rev. Lett. **117**, 097002 (2016).

[47] Z.-X. Li and H. Yao, Edge stability and edge quantum criticality in two-dimensional interacting topological insulators, Phys. Rev. B **96**, 241101(R) (2017).

[48] X.-J. Yu, S.-H. Shi, L. Xu, and Z.-X. Li, Emergence of competing orders and possible quantum spin liquid in SU($n$) fermions, Phys. Rev. Lett. **132**, 036704 (2024).

[49] D. Wang, Y. Li, Z. Cai, Z. Zhou, Y. Wang, and C. Wu, Competing orders in the 2D half-filled SU($2n$) Hubbard model through

the pinning-field quantum Monte Carlo simulations, Phys. Rev. Lett. **112**, 156403 (2014).

[50] M. C. Gutzwiller, Effect of correlation on the ferromagnetism of transition metals, Phys. Rev. Lett. **10**, 159 (1963).

[51] T. M. Rice and K. Ueda, Gutzwiller method for heavy electrons, Phys. Rev. B **34**, 6420 (1986).

[52] D. S. Rokhsar and B. G. Kotliar, Gutzwiller projection for bosons, Phys. Rev. B **44**, 10328 (1991).

[53] H.-K. Jin, H.-H. Tu, and Y. Zhou, Density matrix renormalization group boosted by Gutzwiller projected wave functions, Phys. Rev. B **104**, L020409 (2021).

[54] S. Sorella, S. Baroni, R. Car, and M. Parrinello, A novel technique for the simulation of interacting fermion systems, Europhys. Lett. **8**, 663 (1989).

[55] See Supplemental Material at http://link.aps.org/supplemental/10.1103/PhysRevB.110.085152 for the details of the projective quantum Monte Carlo algorithm and the employment of Gutzwiller projection; details of definition for structure factors; the statistical errors of the Gutzwiller-projection quantum Monte Carlo; systematic comparison of Gutzwiller-projection quantum Monte Carlo with the results of exact diagonalization; and estimation of the total computational time of the Gutzwiller-projection quantum Monte Carlo.

[56] D. P. Arovas, E. Berg, S. A. Kivelson, and S. Raghu, The Hubbard model, Annu. Rev. Condens. Matter Phys. **13**, 239 (2022).

[57] Y. Otsuka, S. Yunoki, and S. Sorella, Universal quantum criticality in the metal-insulator transition of two-dimensional interacting Dirac electrons, Phys. Rev. X **6**, 011029 (2016).

[58] L. Janssen and I. F. Herbut, Antiferromagnetic critical point on graphene's honeycomb lattice: A functional renor-

malization group approach, Phys. Rev. B **89**, 205403 (2014).

[59] K. Ladovrechis, S. Ray, T. Meng, and L. Janssen, Gross-Neveu-Heisenberg criticality from $2 + \epsilon$ expansion, Phys. Rev. B **107**, 035151 (2023).

[60] N. Zerf, L. N. Mihaila, P. Marquard, I. F. Herbut, and M. M. Scherer, Four-loop critical exponents for the Gross-Neveu-Yukawa models, Phys. Rev. D **96**, 096010 (2017).

[61] F. Parisen Toldin, M. Hohenadler, F. F. Assaad, and I. F. Herbut, Fermionic quantum criticality in honeycomb and $\pi$-flux Hubbard models: Finite-size scaling of renormalization-group-invariant observables from quantum Monte Carlo, Phys. Rev. B **91**, 165108 (2015).

[62] Z.-X. Li, Y.-F. Jiang, and H. Yao, Fermion-sign-free Majorana-quantum-Monte-Carlo studies of quantum critical phenomena of Dirac fermions in two dimensions, New J. Phys. **17**, 085003 (2015).

[63] L. Wang, P. Corboz, and M. Troyer, Fermionic quantum critical point of spinless fermions on a honeycomb lattice, New J. Phys. **16**, 103008 (2014).

[64] Z.-X. Li, Z.-Q. Wan, and H. Yao, Asymptotic sign free in interacting fermion models, arXiv:2211.00663.

[65] S. Sorella, Systematically improvable mean-field variational ansatz for strongly correlated systems: Application to the Hubbard model, Phys. Rev. B **107**, 115133 (2023).

[66] R. Levy, M. A. Morales, and S. Zhang, Automatic order detection and restoration through systematically improvable variational wave functions, Phys. Rev. Res. **6**, 013237 (2024).

[67] Y. Chen, L. Zhang, W. E, and R. Car, Hybrid auxiliary field quantum Monte Carlo for molecular systems, J. Chem. Theory Comput. **19**, 4484 (2023).